CO–PROX reactions on copper Y2O3-ZrO2 catalysts prepared by a single step co-precipitation technique

Olivier Marie, Xavier Portier, Nadiia Korsunska, Larysa Khomenkova

CO–PROX reactions on copper Y_2O_3-ZrO_2 catalysts prepared by a single step co-precipitation technique

Olivier Marie[a] ‡, Xavier Portier[b], Nadiia Korsunska[c], Larysa Khomenkova [c,d]

[a] Normandie Univ, ENSICAEN, UNICAEN, CNRS, *LCS*, 14000 Caen, France

[b] CIMAP, CEA, UMR Centre National de la Recherche Scientifique 6252, ENSICAEN, Normandie

[c] V. Lashkaryov Institute of Semiconductor Physics of the National Academy of Sciences of Ukraine, 45 Pr. Nauky, Kiev 03028, Ukraine

[d] National University of Kyiv-Mohyla Academy, 2 Skovorody str., Kiev 04070, Ukraine

Email: olivier.marie@ensicaen.fr, phone: + 33 231 452 825

‡ Corresponding author

Abstract

Nano-sized CuYZr ternary oxides obtained through an original single step co-precipitation synthesis were submitted to an in depth characterization and further tested in the catalytic CO PROX reaction. The tetragonal phase was identified as the main one whatever the calcination temperature. The study of the copper distribution within the crystals through complementary STEM EDX chemical mapping, UV-Vis and H_2 Thermo Programmed Reduction (TPR) analysis allowed the identification of at least three distinct sites. The PROX tests revealed interesting properties with CO conversion as high as 95% and relatively high O_2 selectivity towards CO_2 in the high temperature range. Finally, interesting relationships between relative abundance of copper sites and catalytic activity/selectivity were obtained allowing suggesting relevant active sites.

Key words: CO PROX, Yttrium stabilized zirconia, Copper active sites

1. Introduction

Reaching a high purity of hydrogen stream with a typical maximum level of about 10 ppm of CO is a prerequisite for both ammonia production plants and fuel cell applications. For that purpose, many works have been carried out during the last decades focusing on CO selective oxidation in excess hydrogen (or CO PROX), considered as the simplest and cost effective process to meet the target [1, 2]. The most common operating temperature range for PROX lies between room temperature and 200°C since it also corresponds to the optimum temperature for alkali fuel cells, phosphoric acid fuel cells (PAFC) or proton

exchange membrane (PEMFC) fuel cells [3, 4]. In such cases, a configuration with an upstream PROX unit coupled to the fuel cell is efficient. However, recent developments in molten carbonate fuel cells (MCFC) or solid oxide fuel cells (SOFC) [5] have opened the range towards higher operating temperatures at which the PROX catalysts should remain selective while both the reverse water gas shift (RWGS) and/or CO methanation reactions would consume H_2.

Concerning the nature of the catalytic phase, a typical approach consisted in testing the formulations known to be efficient in CO oxidation in the absence of H_2 excess. Noble metals together with transition metal supported onto various oxides were thus exhaustively tested. Dealing with a non reducible support, it was for example established that CO oxidation over Cu vs Pd supported onto Al_2O_3 showed a higher turnover frequency for the Cu sites [6] thus making the later sites those with the highest intrinsic activity. More generally, the advantages and drawbacks of noble metals and transition metal oxides in PROX have been reported elsewhere [7]. In this review, the authors conclude, even if the influence of water and CO_2 in the reactant stream is not always taken into account, that from a general point of view, transition metal oxide and gold-based catalysts exhibit a better selectivity in a large range of temperature than other noble metal catalysts. As a consequence, recent works mostly focused on Cu and Au based formulations.

As far as gold is concerned, one should remind that starting from the pioneer work by Haruta [8] providing evidence of CO conversion into CO_2 at temperature as low as 200 K, the research on catalytic properties for gold has increased exponentially. In order to get its best oxidation efficiency gold is often coupled with a red-ox support such as ceria [9, 10]. The effect of both the reaction exothermicity and the nanometer-scale gold particle size on CO oxidation and PROX have also been reported [11] while recent advances in preferential oxidation of CO in H_2 over gold catalysts are found elsewhere [12].

Focusing now on the copper based formulations, it is worth noting that the association with ceria as a support is also widely reported. For example, the characterization of active sites/entities and redox/catalytic correlations in copper-ceria based catalysts for PROX was described [13] while other works focused on the influence of the exposed face present in the CeO_2 support on the performance of CuO/CeO_2 catalysts [14]. More recently, the fine structuring of a CuO/CeO_2 catalyst was proposed as an option to improve its performance towards CO-PROX [15]. For this purpose distinct strategies were applied and among them the switch from a classical preparation method involving impregnation of ceria to the direct co-precipitation of the two components within reverse microemulsions led to the obtention of nanostructured oxidised copper-cerium catalysts with varying copper loadings [16, 17].

In the context of oxidation catalysts, knowledge has also been accumulated for decades in the frame of three ways catalysts (TWC) efficient for gasoline engine exhaust gas purification. The optimum formulation of a TWC is based on ceria-zirconia mixed oxides [18, 19] where the solid solution allows faster active oxygen availability. Copper loaded mixed oxide supports containing Zr were thus also tested and the catalytic activity results revealed significant support effects affecting the conversion of either CO or H_2 as well as the selectivity for the CO-PROX process [20]. Indeed, too high active oxygen species may

lead to simultaneous CO and H_2 oxidation. An alternative approach thus consisted in switching from a red-ox (such as ceria) oxide based support to an acidic support that would also favour oxidation reaction but through CO activation rather than O_2 activation. Accordingly, copper/zirconia catalysts were prepared by classical impregnation method whose characterization showed that highly dispersed copper (II) oxide and bulky copper (II) oxide coexist [21]. Later on, Cu/ZrO_2 catalyst prepared via a similar conventional impregnation illustrated that the tetragonal zirconia support presents better CO oxidation activity (not in PROX condition) than the catalyst with the monoclinic support [22]. Aiming at clarifying this structural effect, Cu/ZrO_2 catalysts with amorphous, monoclinic and tetragonal zirconia as supports were prepared and characterized. It was indeed found that zirconia polymorphs had a great influence on the interaction of Cu and ZrO_2. Tetragonal ZrO_2 phase supported copper catalyst showed the highest copper dispersion and confirmed to exhibit better catalytic properties [23]. However, in the temperature range of interest for CO PROX, the stable zirconia phase is the monoclinic one and the metastable zirconia tetragonal phase of interest for catalysis must be stabilized.

Subvalent additives such as yttrium, calcium, scandium, cerium, etc. usually stabilize tetragonal ZrO_2, being yttrium the most common stabilizing agent [24, 25]. Yttria-stabilized zirconia catalysts with different copper contents (2−10 wt % of Cu) were thus prepared by an impregnation technique. The structure and state of the active component-copper species were investigated but no catalytic tests were reported [26]. Concerning the ternary Cu/Y/Zr oxide system, one should also take into account that the superficial Y concentration may also affect the oxygen surface exchange kinetic and thus impact the catalytic efficiency. Indeed, in the context of solid oxide fuel cell, it was recently reported that engineering the surface doping concentration with Y of a common oxide electrolyte, yttria-stabilized zirconia (YSZ), with the help of atomic layer deposition (ALD) led to a 5-fold increase in the oxygen surface exchange coefficient [27]. Moreover, impurities such as copper also induce modification of the $YZrO_2$ structural properties [28]. In fact a previous work on Cu/Y/Zr samples showed that samples, calcined at T_c = 500–700 °C, contain the tetragonal ZrO_2 phase predominantly. However, the increase of T_c results in its transformation to monoclinic one, and the phase transformation happens at higher temperature at higher Cu content [29].

As reported above no exhaustive investigation on PROX catalytic activity of Cu/Y/Zr oxides were reported up to now while such a formulation may lead to interesting results. Only a recent paper showed that an original and cost effective co-precipitation synthesis together with a control of both the calcination temperature and Cu loading allowed the obtaining of PROX efficient catalyst [30]. The present work thus aims at: i) using a similar single step synthesis procedure but using a distinct zirconium source i.e. nitrates instead of oxychlorides; ii) performing a detailed analysis of both the catalyst structure, morphology, texture and red-ox properties, and iii) performing PROX catalytic tests with the goal to establish superficial sites/catalytic activity relationships.

2. Experimental part

2.1. Catalyst preparation

The 3 mol.% Y_2O_3-ZrO_2 nano-powders doped with Cu were prepared according to an original co-precipitation synthesis using Zr, Y and Cu nitrates as precursors, thus avoiding traces of residuals chloride species after annealing. Two distinct initial molar ratio were used $Zr(NO_3)_2$:$Y(NO_3)_3$:$Cu(NO_3)_2$=96:3:1 and 89:3:8 that were further dissolved in distilled water. Starting from such an initial composition, CuO loadings of 1 or 8 mol.% were obtained. Complementary details on the synthesis procedure were previously reported [29]. The xerogels were typically further calcined at T_c=600 and 800 °C for 2h and cooled slowly in the furnace. The samples are further called *x*%Cu–YZr-*y* where *x* stands for the copper molar concentration (mol. %) and *y* is the annealing temperature (°C) respectively.

2.2. Characterization techniques

2.2.1 X-ray diffraction

XRD data were collected in the range of 2θ=20-80° using a Thermo Scientific ARL X'TRA diffractometer with $Cu_{K\alpha}$ radiation (λ=0.15418 nm) in Bragg Brentano geometry.

2.2.2 HRTEM observations and STEM EDX data

The structural properties of the powders were studied by conventional and high-resolution (HR) TEM and Scanning Transmission Electron Microscopy (STEM) combined with EDX. The powders were mixed with ethanol and a drop of the mixture was poured on a 300-mesh holey carbon nickel TEM grid. TEM observations were performed using a double corrected cold FEG ARM200F JEOL microscope operated at 200 kV. The chemical maps were obtained with a CENTURIO JEOL spectrometer attached to the microscope. The STEM EDX chemical maps resolution was 256×256 pixels with a 5 ms exposure time for each spot during the scanning process. The maps were acquired with an acquisition rate of approximately 1000 counts per second and a dead time lower than 10%.

2.2.3 Textural analysis

The catalysts specific area and porosity were investigated by analysis of N_2 adsorption isotherms measured at 77 K using a high-resolution 3-Flex analyser from Micromeritics. Both adsorption branch and desorption branch were measured within the [2.0 10^{-3} – 0.98] relative pressure (P/P°) range.

2.2.4 UV spectroscopy

Diffuse reflectance spectra were recorded with respect to the $BaSO_4$ standard at room temperature by means of double-beam spectrophotometer UV-3600 UV-Vis NIR (Shimadzu Company) equipped with an integrated sphere ISR-3100. Obtained spectra were transformed in absorption ones using standard program

based on the Kubelka-Munk ratio $f(r_\infty) = \frac{(1-r_\infty)^2}{2r_\infty} = \frac{K}{S}$, where $f(r_\infty)$ is the Kubelka-Munk function, $r_\infty = R_{sample} / R_{BaSO_4}$ is the relative diffuse reflection from the sample, while K and S are absorption and scattering coefficients of the sample, respectively.

2.2.5 Temperature Programmed Reduction (TPR) and Oxidation (TPO)

The catalysts red-ox properties were evaluated both qualitatively and quantitatively by submitting them to a reactive gas under increasing temperature after a preliminary pre-treatment was performed.

The catalysts reducibility was investigated under TPR conditions up to 600°C using a flow made of 1250 ppm H_2/Ar (total flow about 50 mL.min^{-1} for 30 mg catalyst) after a preliminary oxidation was operated under 10.5 % O_2 up to 500 °C.

The catalyst was then cooled down under reducing flow till about 50 °C, purged with pure Ar before the subsequent TPO up to 600 °C was performed under similar conditions but substituting H_2 by O_2. In both TPR and TPO, the heating rate was set to 5 K.min^{-1}.

2.3. Catalytic tests

The catalysts efficiencies in PROX were evaluated under flow conditions using a fixed bed reactor configuration. The catalyst particles previously sieved between 100 and 200 μm were homogeneously diluted with SiC with similar mean particles size and located in the central part of a vertical stainless steal reactor possessing a 0.51 cm inner diameter. The weight of catalyst was always about 30 mg while the amount of SiC was adjusted in order to always get a 1.0 cm height catalytic bed. The typical total reaction flow used was set to about 100 mL.min^{-1} thus leading to a typical space velocity of about GHSV = 30 000 h^{-1}.

Generally no pre-treatment of the sample was performed before the catalytic test was run. However, in order to study a possible impact of either oxidative or reducing pre-treatment on the catalysts efficiency/selectivity, activations under a flow made of either 10% O_2 or 10% of H_2 in Ar at about 500 °C during 30 minutes were performed.

Programmed Reaction study of the catalyst activity was then performed between 100 and 600 °C at a 10 °C.min^{-1} heating rate. The reaction flow made of 1.0 % CO, 10.5 % H_2 and 1.5 % O_2 in Ar was established by mass flow controllers and its stability checked by Mass Spectrometry (Quadrupole Pfeiffer Omnistar GSD 301) before switching via a six ways valve to the fixed bed reactor for catalytic reaction.

The analysis of the gas at the outlet of the reactor was achieved simultaneously by IR spectroscopy (Thermo Nicolet NEXUS 670 FTIR equipped with a MCT detector) and Mass Spectrometry (Quadrupole Pfeiffer Omnistar GSD 301). The former measures the CO and CO_2 concentrations while the latter complementary provides O_2, H_2 and H_2O concentrations.

3. Results and Discussion

As described in the introduction part, the nature of the zirconia phase plays a key role on both the copper dispersion and the catalytic activity in CO oxidation. As a consequence, a preliminary step consisted in the identification of the crystalline structure and their relative amount when relevant.

3.1. Structural properties: XRD analysis

XRD patterns of 1%Cu–YZr and 8%Cu–YZr samples, annealed at 600 and 800 °C are shown in **Figure 1** (a) in the range 2θ=20-80°. Peaks at 2θ=30.4°, 35.5°, 50.5°, 73.05°, 74.58° correspond tetragonal (*t*) ZrO_2 phase (JCPDS 80-0784), while for the cubic (*c*) ZrO_2 phase they can be observed at 2θ=30.33°, 35.16°, 50.58° and 74.33° (PDF#01-071-4810). Obviously, most of the peaks resulting from tetragonal and cubic phases are close to each other. Therefore, to discriminate unambiguously these phases, the peaks in the range of 2θ=73-75° are usually used [31-33] because cubic ZrO_2 phase shows in this range only a single peak (at 2θ~74.33°), while the tetragonal phase demonstrates two peaks (at 2θ~73.05° and 74.58°). Since XRD peak positions depend on the doping [31, 34], further analysis of XRD patterns will be performed for this specific range taken into account the number of XRD peaks only.

As one can notice, the 1%Cu–YZr and 8%Cu–YZr samples calcined at 600 °C show only one peak (**Figure 1** b) and a dominant contribution of the cubic phase could thus be assumed. At the same time, an alternative explanation consists in the presence of small size tetragonal nanocrystals. In the latter case, the absence of two peaks that are the feature of tetragonal phase may arise from peaks broadening and their strong overlapping. A clear identification of pure cubic phase from the number of peaks in this 2θ diffraction range is thus hampered when dealing with nanosized crystals. The decrease of their sizes will cause also broadening of the XRD peaks. A more detailed analysis, however, reveals an asymmetric shape of the peak in the 2θ~73-75° range, thus suggesting a rather significant contribution of the tetragonal phase. Consequently, the main contribution to XRD patterns of 1%Cu–YZr and 8%Cu–YZr samples calcined at 600˚C is proposed to arise from a tetragonal phase. This conclusion was supported by Rietveld analysis [31, 34].

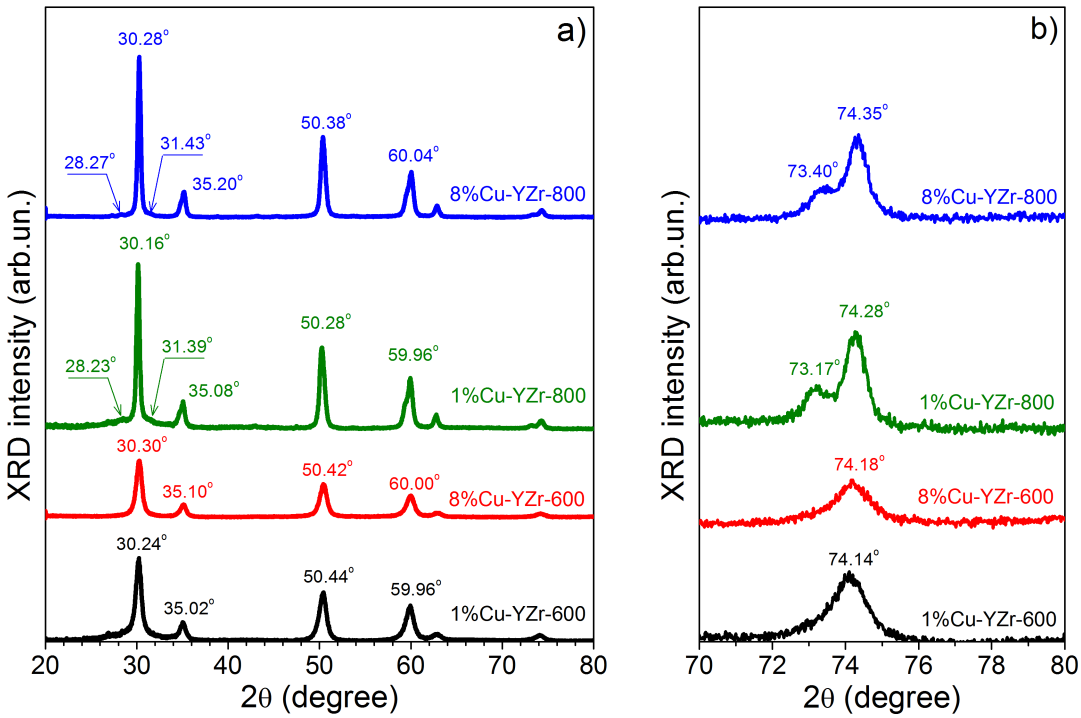

Figure 1: XRD patterns in the range (a) 2θ=20-80° and (b) 70-80° of 1%Cu–YZr and 8%Cu–YZr samples annealed at 600 and 800°C.

Focusing now on the samples annealed at 800°C, the appearance of a small peak at 2θ~28° testifies to the presence of a low amount of monoclinic phase (JCPDS 37-1484). Its contribution estimated by reference intensity ratio (RIR) method using the peaks at 2θ~30° (for tetragonal and cubic phases) and at 2θ~28° (for monoclinic phase) is ~3%. As a conclusion, the tetragonal phase gives the main contribution in all samples investigated, as summarized in **Table 1**.

The coherent domain size was also calculated from peak broadness and the results are reported in **Table 1**. The mean size is consistent with nanocrystals for both samples and the increase of the calcination temperature from 600°C to 800°C obviously leads to soft particles sintering, the coherent domain size remaining at about 25 nm.

Annealing temperature / °C	**1%Cu–YZr**		**8%Cu–YZr**	
	Phase content / %	**Coherent domain size / nm**	**Phase content / %**	**Coherent domain size / nm**
600	97 (T) 3(C)	14	97 (T) 3(C)	13
800	3M-97T	24	3M-97T	26

Table 1. Relative contributions of the different crystalline phases and coherent domain sizes in 1%Cu–YZr and 8%Cu–YZr samples.

In a second step, the structure and chemical composition at the crystal level were analysed by transmission electron microscopy. The results are presented in the following section.

3.2. Crystal size and chemical analysis: TEM study

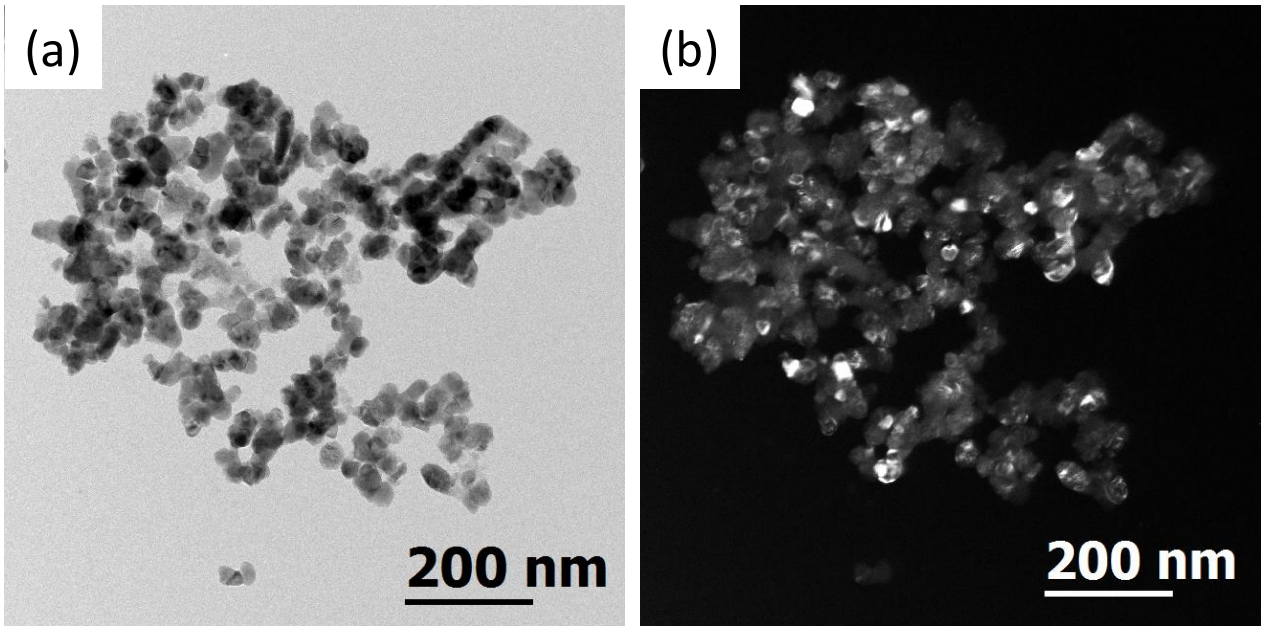

Figure 2: (a) Bright and (b) dark fields TEM images of 8%Cu–YZr-800.

The focus was put on the 8%Cu–YZr-800 samples that, due to its high Cu loading and annealing temperature, is supposed to possibly present 'large' copper clusters. **Figure 2**(a) shows a typical bright field TEM image of some Y-ZrO_2 crystallized grains. The dark Bragg contrasts testify of the crystalline nature of the particles. The bright contrasts observed in the dark field TEM image (Figure 2(b)) confirms this statement. The grain size varies from 15 up to 70 nm with a mean size of about 34 nm (from a measurement of about 20 grains) that is consistent with the coherent domain size estimated by XRD.

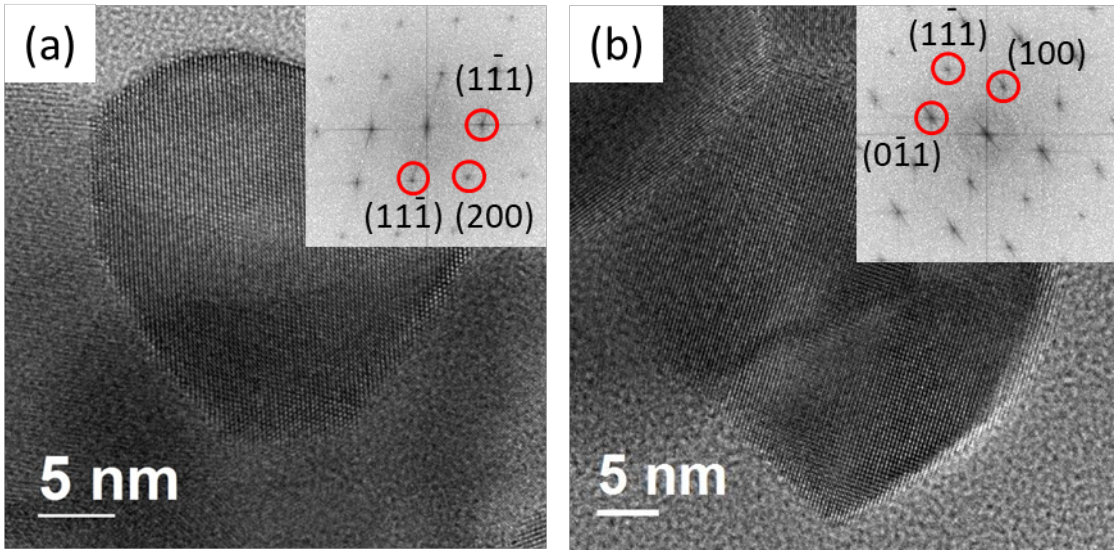

Figure 3: (a) HREM images of 8%Cu–YZr-800 grains with (a) cubic and (b) tetragonal structures. The corresponding FFTs are shown in inset.

HREM images have also been taken (**Figure 3**) to show that the grains are mainly single crystalline and one example of each structure of zirconia is reported in **Figure 3** (a) for cubic and in **Figure 3** (b) for tetragonal. The insets are the corresponding Fast Fourier Transforms (FFTs) that are consistent with [011] projections of cubic and tetragonal structures. No monoclinic structure has been observed in agreement with the low proportion of this phase in the powder for this sample.

Chemical mapping has been further carried out using the STEM EDX technique. A series of maps are presented in **Figure 4** as well as the corresponding STEM HAADF image that reveals the presence of darker regions in the grains (**Figure 4**(a)). Since the contrast of this image is based on the Z value of the elements present in the grains (the higher mean Z value, the brighter the contrast), one can assume that these darker regions are voids or cavities with a mean size of about 10 nm. Some of them have facets parallel to dense planes of zirconia. It is worth noting that all single crystalline grains present several cavities. The other interesting feature is the presence of copper enriched particles (**Figure 4**(e)). These clusters of a few tens of nanometers in size are most probably copper oxides.

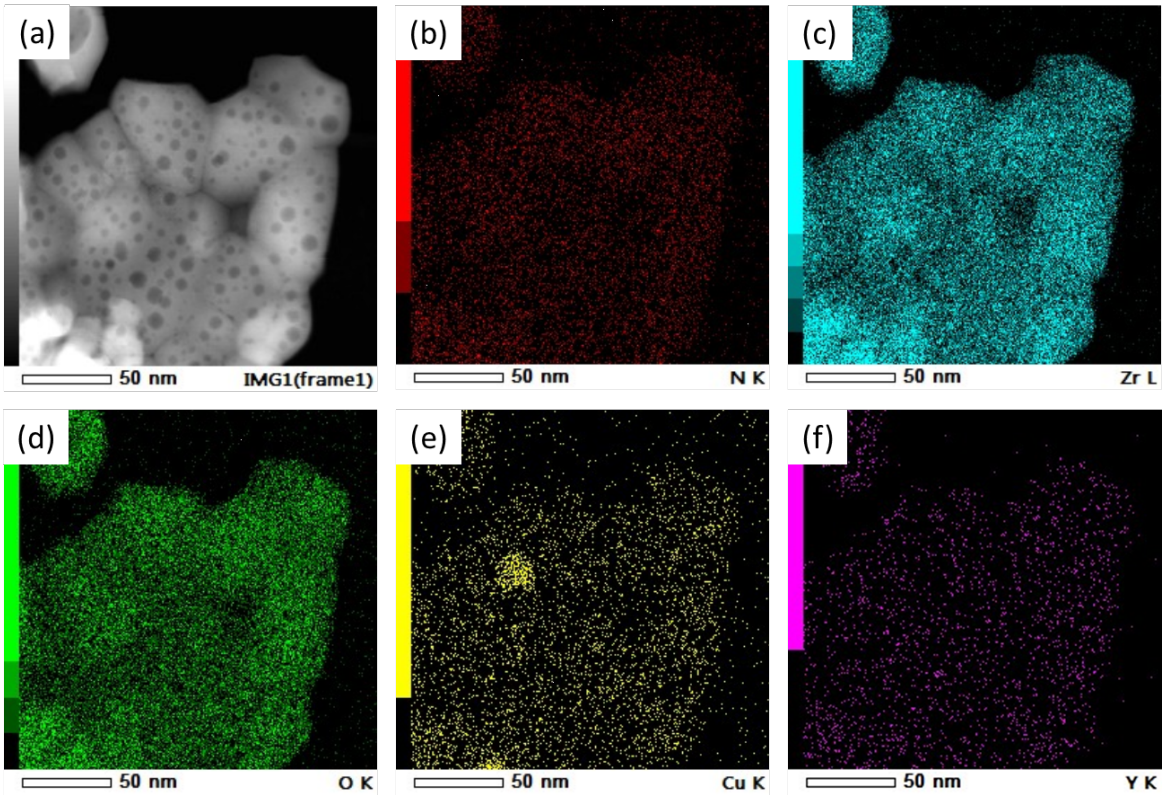

Figure 4: (a) STEM HAADF image of large 8%Cu–YZr-800 grains; STEM EDX chemical maps corresponding to N (b), Zr (c), O (d), Cu (e) and Y (f) elements.

Aiming at locating copper in the powder, a complementary EDX analysis was performed. **Figure 5**(a) is a STEM HAADF image showing various 8%Cu–YZr-800 grains with high amount of boundaries between them. An EDX profile has been performed from one grain to the middle of the adjacent one (**Figure 5**(b)) and it revealed an increase of copper content at the level of the grain boundary suggesting a

Cu diffusion out of the grains. This result is consistent with the presence of copper rich clusters in the 8%Cu–YZr-800 sample together with cavities inside the zirconia structure where Cu sites were initially present.

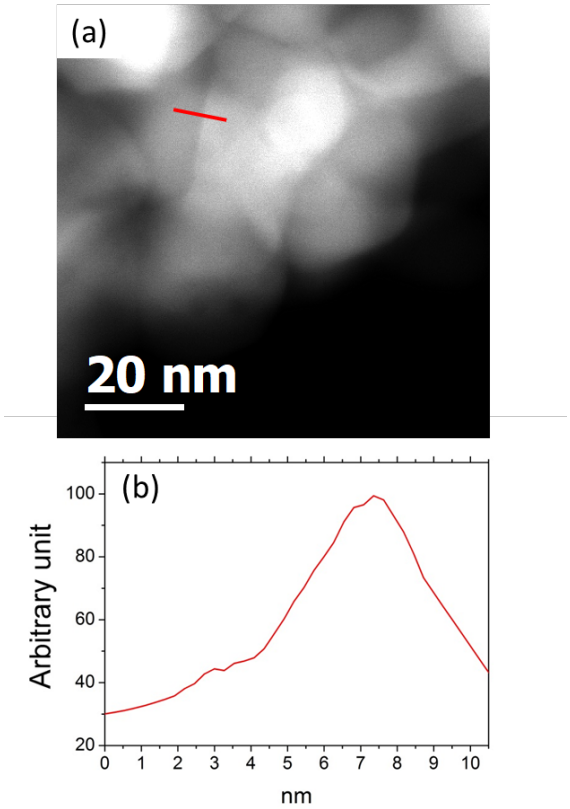

Figure 5: (a) STEM HAADF image of a few 8%Cu–YZr-800 grains with grain boundaries; (b) EDX profile of copper along the line shown in (a) and crossing a grain boundary.

A next step required before studying the catalysts activity consists in the characterization of their superficial properties.

3.3. Textural properties: N_2 adsorption isotherms

The specific surface area of any given catalyst being of primary importance to provide a high interface between the gaseous reactants and the solid catalysts, this property was first evaluated.

Figure 6 presents the N_2 adsorption isotherms obtained at 77K after a preliminary activation under a vacuum at 400°C.

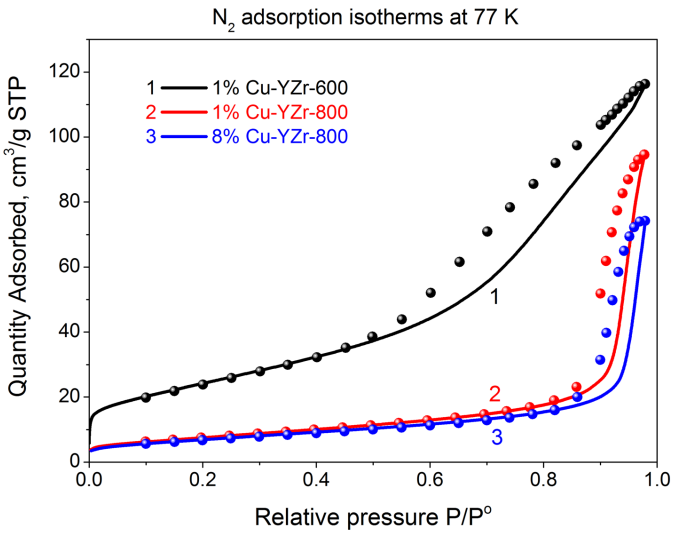

Figure 6: N_2 adsorption isotherms at 77K after pre-treatment under a vacuum at 400°C for samples 1%Cu–YZr-600 (curve 1), 1%Cu–YZr-800 (curve 2) or 8%Cu–YZr-800 (curve 3). Solid curves and corresponding circle symbols show adsorption and desorption branches, respectively..

According to the IUPAC classification recently reviewed [35], the isotherm for 1%Cu–YZr-600 is rather a type IVa one typical for a mesoporous solid with typical mean pore diameter above 4 nm. The absence of horizontal range in the upper level of P/P° however makes it a composite with a contribution of type II isotherm. The hysteresis between the adsorption and desorption branch presents a Type H_3 loop for which the lower limit of the desorption branch is normally located at the cavitation-induced P/P^0. Isotherms obtained after annealing at higher temperature (800 °C) both present a hysteresis loop shifted towards higher P/P_0 characterized by a more vertical shape.

The isotherms analysis according to the BET theory was achieved it the $0 < P/P° < 0.07$ range in order to get values for specific area. The Table 2 summarizes the results obtained. The high decrease of the specific area from 76 to 24 $m^2.g^{-1}$ upon increasing the annealing temperature (T_c) of sample 1%Cu-YZr from 600 to 800°C provides evidence of sintering phenomena. Now comparing the impact of Cu loading at an annealing temperature of 800°C, it appears that moving from 1 to 8 % Cu doping little affects the specific area.

Catalyst	**Specific area BET /$m^2.g^{-1}$**	**Total porous volume / $mL.g^{-1}$**	**Mean pore diameter / nm**
1%Cu–YZr-600	76	0.180	9.4
1%Cu–YZr-800	24	0.145	25
8%Cu–YZr-800	22	0.115	21

Table 2. A summary for the catalysts main textural properties.

Considering the estimation of the porous volume, it is worth reminding that none of the three obtained isotherms possesses a horizontal plateau near P/P°=1. This clearly indicates that not only mesopores but also macropores (> 50 nm) are present for the whole samples, which theoretically prevents the total pore volume (V_p) from accurate measurement. It was however decided here to estimate the total pore volume from the value measured at P/P° = 0.97 (less than 66 nm diameter). The Table 2 then illustrates the drop of the total pore volume upon an increase of T_c from 600 to 800°C for the 1% Cu-YZr catalyst. The comparison of the isotherm shapes obviously reveals that mesoporous volume is lost upon thermal sintering. Focusing now on the Cu loading effect, it seems that the presence of a high amount of copper affects the sintering mechanism. Indeed, a further drop of the total porous volume is noticed for sample 8% Cu-YZr-800.

The mean pore size diameter was estimated according to the very simple cylindrical pore model leading to the following equation:

(Eq.1) $d_{mean} = 4\ V_p / S_{BET}$

Values reported in Table 2 are consistent with an increase of the macropores contribution upon an increase of the calcination temperature. A further confirmation was provided when studying the pore size distribution from the adsorption branch according to the BJH model. In fact, the model was only reliable for the 1% Cu-YZr-600 catalyst. In this case the $dV/dd_{mean} = f(d_{mean})$ plot (not shown) presents a rather sharp pore size distribution centred at about 8 nm that is consistent with the value reported in Table 2 and with no contribution of pore diameter above 50 nm (macropore). On the contrary, both samples aged at 800°C leads to broad pore size distribution curves with maximum values (30 nm and 43 nm for 1% Cu-YZr-800 and 8% Cu-YZr-800, respectively) that do not match anymore with those obtained with the simple cylindrical mesopore model (Table 2). Finally, considering a simple particles packing model for aggregates, the XRD data and textural data are in perfect agreement regarding the thermal effect on the 1%Cu–YZr. Indeed, the highest annealing temperature leads to the highest coherent domain size (**Table 1**) thus related with the highest mean pore diameter (void volume in the grain packing model).

3.4. Optical properties: UV-Vis analysis

UV-Vis diffuse reflectance (DR) spectra of 1%Cu–YZr and 8%Cu–YZr samples annealed at 600 and 800°C are shown in **Figure 7**. These DR spectra contain an absorption band (peak at ~270 nm) close to the ZrO_2 band edge. Its intensity is higher for 8%Cu–YZr samples. This band was more precisely identified to arise from light absorption by oxygen vacancies [28]. Since Cu lattice incorporation results in oxygen vacancies formation [28], the higher intensity of the 270 nm band in the 8%Cu–YZr samples reveals a higher content of oxygen vacancies due to a higher Cu content in the ZrO_2 lattice.

Regarding the heating effect, the intensity of this oxygen vacancy band only slightly decreases with an annealing temperature increase from 600 to 800°C when 1%Cu–YZr sample is concerned. A much more pronounced decrease is noticed with 8%Cu–YZr samples.

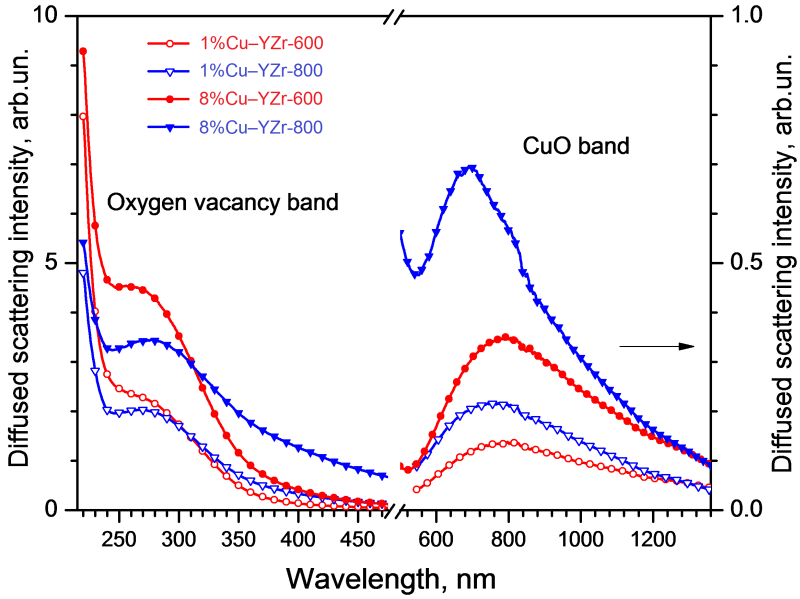

Figure 7: UV-Vis diffuse reflectance spectra of 1%Cu–YZr and 8%Cu–YZr samples annealed at T_c=600 and 800˚C.

In addition to the absorption near ZrO_2 band edge, a second broad band is observed in the 600-900 nm range. Its intensity is again higher with 8%Cu–YZr samples but this time an increase is noticed upon an increase of the annealing temperature, being accompanied by a shift of peak position to lower wavelengths. Bands in this 600-900 nm range are usually assigned to *d-d* transitions of the Cu^{2+} ions in an octahedral or tetragonal distorted octahedral surrounding [26] and associated either with dispersed CuO on the surface of nanocrystals [36] or with Cu_{Zr} substitutional atoms located in the near-surface region [26, 37]. The intensity increase of this d-d transition bands at the expense of the oxygen vacancy band intensity at high annealing temperature is observed for both Cu loading, the phenomenon being more noticeable at high Cu loading. This result is consistent with Cu migration out form the zirconia framework upon increasing the annealing temperature, as previously suggested form TEM chemical mapping. This Cu out migration is limited when only 1% Cu is present while for 8wt% Cu loading 'big cavities' are observed within the ZrO_2 crystal (**Figure 4**(a)). These cavities observed with 8%Cu–YZr-800 were related with high Cu concentration at the grain boundaries (**Figure 5**(b)) thus suggesting that Cu out diffusion till the external area of ZrO_2 particles may then proceed. Moreover, the increase of Cu loading not only provokes an increase of the d-d transition band intensity but also a marked low wavelength shift upon heating from 750 to 700 nm. This shift was attributed to an increase of the octahedral distortion [26, 36], which was ascribed to the deformation of surface CuO chains [26]. This latter result clearly indicates that not only the amount of extra-framework Cu sites is much higher for the 8%Cu–YZr-800 sample but also that the nature of these Cu_xO_y species present at the surface is distinct.

A more careful look at the redox properties of these various Cu species was thus undertaken for the 8%Cu–YZr-800 sample that obviously presents the highest heterogeneity of sites.

3.5. Red-ox properties: H_2 TPR and O_2 TPO over 8%Cu-YZr-800

The textural characterization is important in order to get an estimation of the access towards superficial sites, while the UV-Vis analysis confirmed the presence of various Cu_xO_y species on the surface of YZr nanocrystals. Nevertheless, the complementary evaluation of their related red-ox properties involved in CO PROX reaction is also a prerequisite. For this purpose, both Thermo Programmed Reduction (TPR) and Oxidation (TPO) were performed in order to investigate the nature of the active sites and their amount. As reported above, the 8% Cu-YZr-800 catalyst possesses the highest heterogeneity of Cu sites but also as described in the next 3.6 section this catalyst yields the best CO PROX efficiency in the low temperature range. As a consequence, the focus was put on this sample.

Before TPR was performed, the catalyst was oxidized under 10.5% O_2 up to 500°C aiming at providing fully oxidized CuO as a starting state, in agreement with previous investigations [16, 17, 38, 39]

The upper part of Figure 8 represents the mass-spectrometry (MS) signals obtained for H_2 (m/z=2) and H_2O (m/z =18) during the TPR analysis realized at a heating rate of 5 $K.min^{-1}$ under 1250 ppm H_2 with a final isotherm at 600°C for about 45 min.

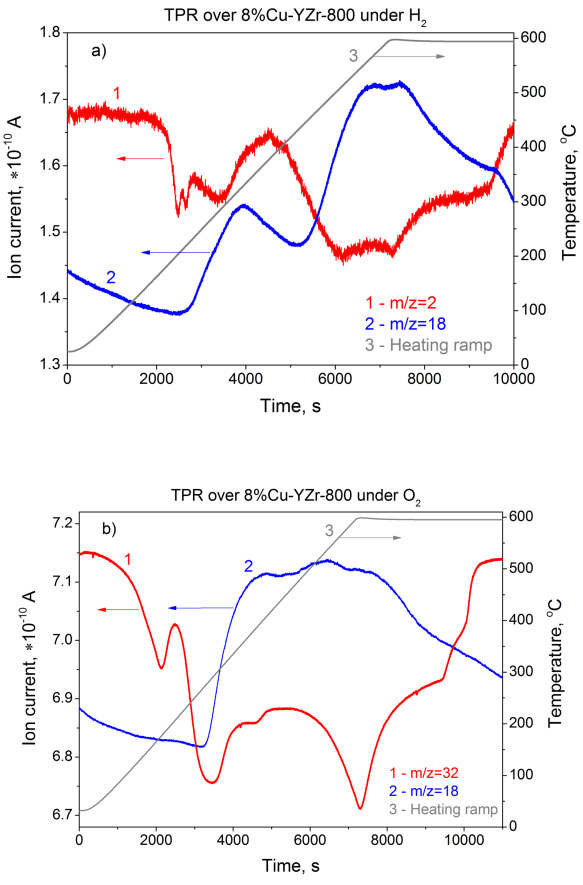

Figure 8: (a) TPR of 8%Cu–YZr-800 catalyst under 1250 ppm H_2/Ar after a pre-treatment under O_2 at 500°C. (b) Subsequent TPO after cooling down to about 50°C under 1250 ppm H_2/Ar. The MS signals at m/z = 2 and 18 stand for H_2 and H_2O respectively. The MS signal at m/z = 32 typical for O_2 was divided by 25 in order to get common scale for both TPR and TPO.

The H_2 consumption can be split in three distinct temperature ranges: zone 1 for which 160°C < T < 240°C, zone 2 for which 240°C < T < 375°C and zone 3 for which 375°C < T < 600°C. The zone 1 presents two sharp peaks whose minima lie at T= 202°C and 218°C. The rather low temperature at which the copper reduction starts in zone 1 suggests that the corresponding sites could be highly dispersed copper oxide oligomeric species Cu_xO_y located at the outside surface of the catalyst [21] and related to the UV-Vis band at 750 nm. As recently discussed by Gamarra et al [14], it is hard to distinguish whether the two consecutive low temperature peaks characterize distinct sites with slightly different reducibility or consecutive steps for reduction of one single type of sites. Indeed, copper oxide reduction may proceed according to the following sequence:

$$\text{(Eq.2)} \qquad 2\,CuO + H_2 \rightarrow Cu_2O + H_2O$$

$$\text{(Eq.3)} \qquad Cu_2O + H_2 \rightarrow 2\,Cu + H_2O$$

The analysis of the stoichiometry for Eq.2 and Eq.3 indicates that the elemental Cu/H_2 ratio is identical. Taking into account that both peak shape and intensity at 202°C and 218°C are similar, the amount of consumed H_2 is thus also identical. As a consequence, the hypothesis of consecutive steps for reduction of one single type of copper superficial site would here be preferred. A more quantitative approach was performed through transformation of the MS signal into H_2 molar fraction thanks to a calibration curve and further integration of the area of missing H_2. Considering the total flow and the weight of catalysts, values for consumed H_2 (in $mol.g^{-1}$) were calculated for each temperature zone. The Table 3 summarizes the obtained values.

	TPR / TPO zone 1: 160 < T < 240°C zone 1': 40 < T < 210°C	**TPR / TPO zone 2: 240 < T < 375°C zone 2': 210 < T < 410°C**	**TPR / TPO zone 3: 375 < T < 600°C zone 3': 410 < T < 600°C**	**TPR / TPO total**
Consumed H_2 / $mol.g^{-1}$	$9.53\ 10^{-5}$	$1.73\ 10^{-4}$	$9.56\ 10^{-4}$	$1.22\ 10^{-3}$
Consumed O_2 / $mol.g^{-1}$	$6.13\ 10^{-5}$	$2.60\ 10^{-4}$	$5.27\ 10^{-4}$	$8.49\ 10^{-4}$

Table 3. A summary for the 8%Cu–YZr-800 catalyst TPR/TPO analysis.

The amount of easily reducible sites (T <240°C) for 8%Cu–YZr-800 would thus represent about 8% of the total reducible sites. It is worth noting that the m/z=18 signal typical for water production does not allow to evidence the two consecutive steps described by Eq. 2 and Eq. 3. The water detection is not only

delayed to higher temperature but also the two expected peaks are not separated. Only one first broad peak is observed between 225°C < T < 425°C thus comprising both zone 1 and zone 2. This most probably arises from water interaction with the catalyst surface in the lower temperature range at which it remains adsorbed while further desorption then progressively proceeds.

The zone 2 for H_2 consumption consists in a broader peak whose minimum lies at about 285°C. This higher temperature clearly indicates a harder reduction of the corresponding Cu sites while the broadness of the peak would reveal a larger distribution of particle size. H_2 TPR peak at very similar temperature (290°C) was previously observed over Cu loaded zirconia and assigned to bulky CuO species [21, 22]. In the present work, this zone 2 is thus tentatively related with the Cu rich zone previously identified in TEM. Part of copper clustering would indeed lead to bigger CuO particles (compared to oligomeric Cu_xO_y species) related with a UV-Vis d-d band at 700 nm, remaining in close contact with the YZr oxide and whose size would however remain in the nanometric range since no typical XRD diffraction peak could be detected. The corresponding amount (Table 3) represents about 14% of the total reducible sites.

The zone 3 for H_2 consumption lies at very high temperatures to account for Cu_xO_y reduction only. Indeed, it was observed by Zhou et al that after being treated by H_2-TPR, the crystalline CuO diffraction peaks disappear, whereas diffraction peaks of Cu° are produced within the 50-500°C range. Their H_2 TPR data also indicate that pure CuO phase is reduced to Cu° with a peak at temperature below 400°C [22] while in the present work the H_2 consumption peak stands at about 525°C. Moreover the amount of consumed H_2 is this zone 3 is even higher that the total amount of theoretical Cu sites estimated at 6.7 10^{-4} mol.g^{-1} starting from the following initial stoechiometry: $(CuO)_8(ZrO_2)_{89}(Y_2O_3)_{1.5}$. All these data clearly suggest that the YZr support reduction proceeds in this zone 3 temperature range. Very little recent papers report H_2 TPR data for temperatures as high as 600°C, however Shimokawabe [21] in their exhaustive study did study H_2 TPR up to 800°C and included the bare ZrO_2 oxide. They found a broad peak within the 400-600°C range that they assigned to the zirconia reduction. They observed a similar high temperature peak with 8wt%Cu loaded zirconia but with a much lower relative intensity compared to what is observed in our present work. According to the above literature data and our very high relative amount (80%) of consumed H_2 at T> 375°C, we assign the zone 3 to the reduction of the YZr oxide. The Yttrium incorporation inside the lattice is indeed reported to enable the stabilization of a high amount of oxygen vacancies [27].

Aiming at analysing the reversibility of the copper reduction process, the sample was subsequently submitted to TPO. For this purpose, the 8%Cu–YZr-800 catalyst was first cooled down from 600°C to room temperature under the TPR H_2 flow. A purge of the lines under pure Ar until no H_2 was detected at the outlet of the reactor was then performed before the TPO was initiated. The lower part of Figure 8 represents the MS signals obtained for O_2 (m/z=32) and H_2O (m/z =18) during the TPO analysis realized at a heating rate of 5K.min^{-1} under 1015 ppm O_2 with a final isotherm at 600°C for about 60 min. The O_2 consumption can again roughly be split in three distinct temperature ranges: zone 1' for which 40°C < T <

210°C, zone 2' for which 210°C < T < 410°C and zone 3' for which 410°C < T < 600°C. The zone 1' presents only one sharp peak whose minimum lies at T= 175°C, i.e a little earlier than the first peak observed in TPR (202°C). The re-oxidation of copper sites thus appears easier than their reduction. Assuming that the reactivity of Cu sites should follow the same order upon increasing temperature, one should assign the first TPO peak to the re-oxidation of superficial oligomeric reduced Cu sites into oligomeric Cu_xO_y. The expected amount of consumed O_2 to convert Cu into CuO being half that of H_2 for CuO reduction into Cu, the values reported in Table 3 for zone 1 are roughly consistent with the assignment to similar copper superficial sites involved in zone 1 and 1'. Furthermore, the amount of easily oxidized sites (T < 210°C) for 8%Cu–YZr-800 represents about 7% of the total sites that is consistent with the fraction of easily reducible sites (T < 240°C) previously determined (about 8%). The comparison of these quantitative values together with that of the number of peaks detected in zone 1 and 1' strongly suggests that oligomeric superficial CuO species are prone to reduction in two consecutive steps (with Cu_2O intermediate species) while oligomeric superficial Cu° species easily and quickly converts to CuO.

Considering the zone 2' under TPO conditions, its temperature extent is broader than zone 2 under TPR conditions thus indicating that oxygen diffusion towards sub-superficial or bulk sites of nanosized Cu clusters requires higher activation energy. Regarding the higher amount of oxygen consumed in zone 2' compared to H_2 consumed in zone 2, the trend is now opposite to what is predicted from the stoichiometry of Cu oxidation to CuO compared to CuO reduction into Cu. Here, the amount of consumed O_2 highly exceeds the theoretical value. This unexpected result should be related with another unexpected one, i.e the detection of water production upon TPO. Indeed, the m/z = 18 signal typical for H_2O starts to increase above 270°C to reach values of similar magnitude to those observed under TPR conditions (the MS scale for TPR and TPO is common). This point should be clarified by complementary experiments but it appears that some hydrogen source would be stored in/on the catalyst during the previous reduction step.

Considering now the zone 3' ranging from 410 to 600°C, it represents the highest contribution to oxygen consumption and should consequently be related with the lattice refilling of O vacancies preliminary created under H_2 TPR. It is worth noting that the amount of consumed O_2 ($5.27\ 10^{-4}$ mol.g^{-1}) lies within the range typical for oxygen exchange capacity in the 500-700°C temperature domain over YZr [40].

3.6. Evaluation of the performances in the CO PROX reaction

The whole x% Cu-YZr-y series characterized in the previous part was not submitted to catalytic tests but only selected samples were tested.

3.6.1. Comparison of the catalytic activities for selected samples of the the x%Cu–YZr-y series

In a recent paper investigating the thermal evolution of similar samples [34], it was observed that the annealing temperature had a great influence on the evolution of the crystalline structure and dopant distribution. These results were confirmed in the above reported XRD and UV-Vis data that indicate that Cu incorporation in the YZr oxide nanocrystals of tetragonal phase reaches a maximum value at about Tc=600°C for the 1% Cu-YZr-y series. While keeping the tetragonal phase as the dominant one (97%), annealing up to 800°C for the 1% Cu-YZr was shown by UV-Vis (**Figure 7**) to provoke an out diffusion (even if limited) of copper to external sites. As a consequence, it was decided to first focus on the comparative analysis of the catalytic activity for samples 1% Cu-YZr-600 and 1% Cu-YZr-800.

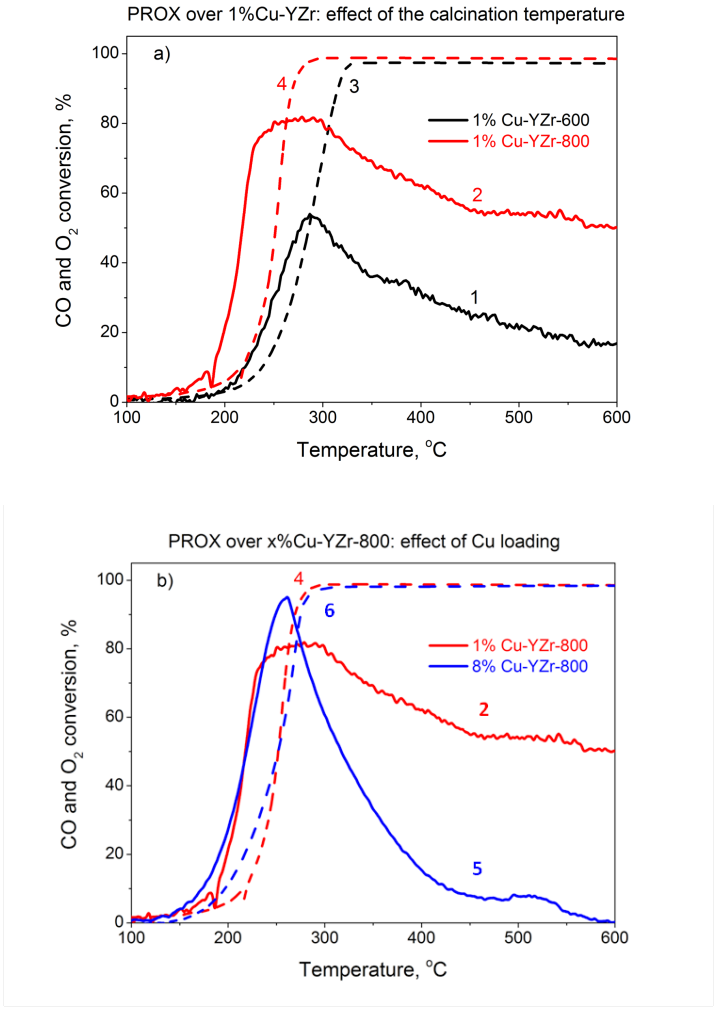

Figure 9: a) Effect of the annealing temperature and **b)** effect of the Cu loading on the CO (solid curves 1, 2 and 5) and O_2 (dashed curves 3, 4 and 6) conversion obtained in PROX conditions made of 1 % CO, 10.5 % H_2 and 1.5 % O_2 in Ar at GHSV = 30 000 h^{-1}. Curves 1, 3 stand for samples 1%Cu-YZr-600; curves 2, 4 stand for samples 1%Cu-YZr-800; curves 5, 6 stand for samples 8%Cu-YZr-800.

Figure 9 (a) reveals that an increase of the annealing temperature from 600°C to 800°C clearly boosts the catalytic efficiency of sample loaded with 1% Cu. Indeed, it is observed a net shift of the conversion curves for both CO and O_2 towards lower temperatures thus making 1% Cu-YZr-800 the most efficient catalyst in the whole tested temperature range. More precisely, the light off (LO) temperature, defined as the lowest temperature at which a 50% conversion level is reached for CO, is 60°C lower for 1% Cu-YZr-800 (T_{LO} = 218°C) compared to 1% Cu-YZr-600 (T_{LO} = 278°C). Moreover, the maximum CO conversion level reached for 1% Cu-YZr-600 only slightly exceeds 50% (54% at 287°C) while value as high as 85% is obtained for 1% Cu-YZr-800 at 275°C. These results point out that copper lattice sites are not good candidate for catalytic sites active for CO oxidation in the low temperature range and as a consequence that out diffusion of copper most probably through interstitial sites provides the superficial active sites. It is also worth noting that the O_2 selectivity toward CO_2 defined as: $S_{O_2 \rightarrow CO_2} = \frac{(CO_{in} - CO_{out})}{2*(O_{2\,in} - O_{2\,out})}$ reaches values above 200% (at about 215°C) for 1% Cu-YZr-800 while reasonable values of about 60% i.e. well below the theoretical limit of 100% are obtained for 1% Cu-YZr-600. In another word, under these transient thermal conditions, the amount of available oxygen species is higher than the gaseous fed O_2. This suggests that some superficial sites are able to store oxygen and quickly release them upon interaction with CO. Such reactive oxygen may be related with the superficial sites responsible for the lowest TPR H_2 peak observed at 202°C and tentatively related with the CuO reduction into Cu_2O. This hypothesis is consistent with the fact that ZrO_2 support is reported to favour Cu^{2+} reduction into active Cu^+, therefore easily forming a redox cycle of Cu^+ to Cu^{2+} [22].

Furthermore, in another recent paper dealing with the study of PROX efficiencies of similar samples prepared from an alternative Zr precursor [30], it was observed that the Cu loading also had a crucial impact on the CO conversion. It was thus decided to also compare the behaviour of samples containing 1 and 8 wt% Cu annealed at the same temperature of 800°C. The Figure 9 (b) clearly indicates that both 1%Cu–YZr-800 and 8%Cu–YZr-800 present similar CO conversion level for PROX temperature up to about 235°C with identical T_{50} values of 220°C. On another hand, a careful look at the O_2 conversion in this low temperature range reveals a shift towards higher temperature for 1%Cu–YZr-800, thus making this catalyst the more selective in CO PROX. Comparing the highest CO conversion level reached, the sample 8%Cu–YZr-800 is slightly better than the 1%Cu–YZr-800 one with a maximum value of 95% at 260°C compared to 85% at 275°C.

The higher selectivity in CO PROX for the 1%Cu–YZr-800 catalyst is further confirmed in the temperature range above 280°C at which the O_2 conversion reaches the 100% level for both samples. Indeed, for T>280°C, the CO conversion drops quickly to values lower than 20% (at about 400°C) for 8%Cu–YZr-800 while it decreases slowly and remains above 50% up to 600°C for 1%Cu–YZr-800. This rather high CO conversion level maintained in the high temperature ranges (associated with O_2 selectivity

of 18% at 600°C) opens up applications for further purification of H_2 stream feeding either Molten Carbonates Fuel Cells (MCFC) or Solid Oxides Fuel Cells (SOFC) whose operating temperatures are typically above 600°C [5]. As a summary, it should be emphasized that a high copper loading is beneficial in the temperature range below 280°C while low copper loading leads to more selective sites for catalytic oxidation of CO that plays a key role to maintain an excellent CO conversion level in the high temperature range.

Regarding the sites showing a high selectivity towards CO oxidation, it is worth reminding that their amount increases upon increasing the annealing temperature from 600 to 800°C for the 1%Cu-YZr samples (Figure 9 a). On another hand, the UV-Vis spectra showed an intensity increase of d-d band typical for superficially dispersed CuO bands at the expense of the oxygen vacancy band intensity upon increasing annealing temperature. These results allow concluding that lattice copper species responsible for oxygen vacancy band should be rejected as selective sites for CO oxidation. On the contrary, oligomeric Cu_xO_y highly dispersed at the YZr surface are good candidates for such selective sites. These sites are responsible for the UV-vis signal at 750 nm (**Figure 7**) and the low temperature TPR doublet at 202-218°C (Figure 8 a). Upon increasing the Cu loading from 1% to 8%, the amount of such selective sites may increase, but the annealing at 800°C also leads to the appearance of Cu oxide clustering as detected by TEM (**Figure 4** and **Figure 5**). The UV-Vis d-d band intensity increase and shift at 700 nm (**Figure 7**) together with the H_2 TPR peak at 285°C (Figure 8 a) are further evidence of the appearance of bulky CuO clusters upon annealing up to 800°C. The number of Cu sites in 'big clusters' is estimated to reach about twice that for 'oligomeric' species (Table 3). As a consequence, for the 8%Cu–YZr-800 catalyst, the CO oxidation selective sites are not the dominant species. The bulky CuO clusters highly contribute to O_2 consumption in the parallel H_2 oxidation thus leading to a pronounced CO conversion drop by lack of available O_2.

3.6.2. Detailed analysis of the 8%Cu–YZr-800 behaviour

One of the priority for the most common CO PROX catalysts is to present high efficiency in the low temperature range in order to be applied for purification of H_2 whose conversion in promising PEMFC and PAFC fuel cells proceeds in an operating temperature range lying between 150-200°C [3, 4]. As a consequence, it was chosen according to the results reported above to focus on the most promising 8%Cu–YZr-800 catalyst.

3.6.2.1. Stability upon cycling.

The study of catalysts under thermo programmed reaction conditions is a fast and reliable tool when comparative ranking is required but these 'out of steady state' conditions do not provide information on the catalyst stability. It is however of primary importance to make sure that no catalyst poisoning or ageing

(leading to lost of activity) proceeds upon time on stream. This point is little often addressed as concluded by Bion et al. [7] but deactivation process have been reported to take place rapidly under the reactant stream for CuO/CeO_2 based formulation [39]. Aiming at testing our Cu/YZr formulation, the PROX test was repeated. The reactor filled with 8%Cu–YZr-800 was kept about one month under ambient air before a second test was performed in exactly similar conditions and without any pre-treatment.

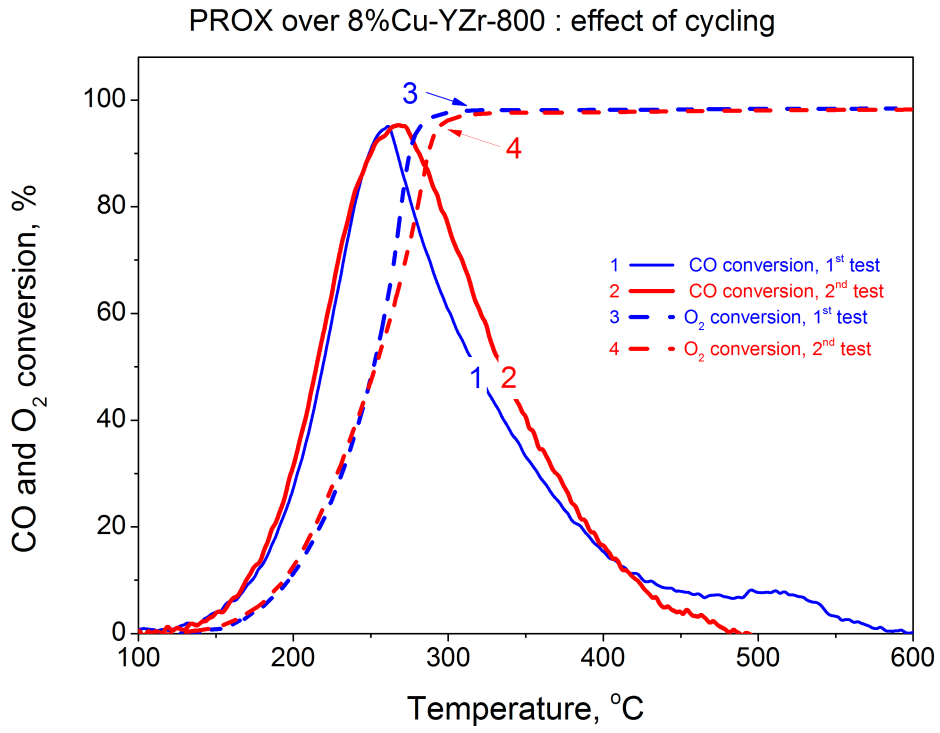

Figure 10: Study of the 8%Cu-YZr-800 catalyst stability upon cycling. CO (solid curves 1 and 2) and O_2 (dashed curves 3 and 4) conversion obtained in PROX conditions made of 1 % CO, 10.5 % H_2 and 1.5 % O_2 in Ar at GHSV = 30 000 h^{-1}. Curves 1, 3 and curves 2, 4 correspond respectively to the first and second tests.

Figure 10 clearly illustrates that both CO and O_2 conversion curves superimpose perfectly at least up to about 260°C. A slight deviation is observed for higher temperatures but the trend is opposite to a deactivation phenomenon. Indeed, the second test leads to both slightly higher CO conversion and lower O_2 conversion in the high temperature range thus indicating that the selectivity towards CO_2 for 8%Cu–YZr-800 increased to a small extent.

3.6.2.2. Influence of a reducing or oxidizing pre-treatment.

As reported above in the 3.6.1 part, the O_2 selectivity toward CO_2 for sample 1% Cu-YZr-800 reaches values above 200% in the low temperature range (at about 215°C). Aiming at understanding this phenomenon and getting more insight into the nature of the involved oxygen species, the effect of either a reducing or oxidizing pretreatment was investigated.

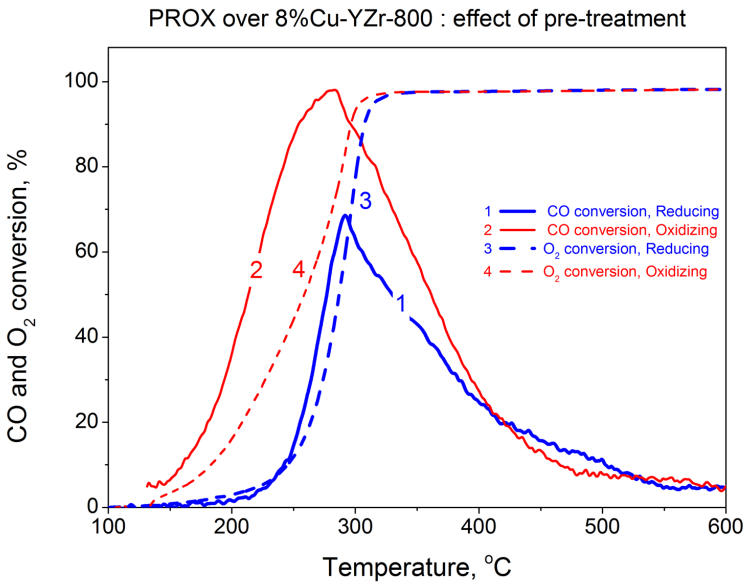

Figure 11: Study of the pre-treatment effect on 8%Cu-YZr-800 catalyst. CO (solid curves 1, 2) and O_2 (dashed curves 3, 4) conversion obtained in PROX conditions made of 1 % CO, 10.5 % H_2 and 1.5 % O_2 in Ar at GHSV = 30 000 h^{-1}. Curves 1 and 3 correspond to a reducing pre-treatment at 500°C under 10.5% H_2 in Ar. Curves 2 and 4 correspond to an oxidizing pre-treatment at 500°C under 10.5% O_2 respectively.

Figure 11 obviously indicates that a reducing pre-treatment has a strong negative impact on both the CO and O_2 conversion. More precisely, for temperature below 200°C the CO conversion remains at a zero level indicating the absence of active oxygen species. The TPO experiment (Figure 8) however showed that after a reducing pre-treatment, the catalyst re-oxidation proceeds at rather low temperature with a first O_2 consumption peak at 175°C. Assuming that in this low temperature range (zone 1 and 1' as defined from Figure 8) the involved sites are oligomeric copper superficial species claimed to be the active and selective sites for CO oxidation, the reaction should have started. In order to explain the absence of CO conversion for T<200°C after a reducing pre-treatment, two distinct hypotheses are proposed. In the first one, it is suggested that under the PROX conditions (compared to TPO conditions), the co-fed H_2 delays the oligomeric Cu° oxidation towards higher temperature thus limiting the amount of active sites for CO oxidation. The second hypothesis considers Cu^+ (from Cu_2O oligomeric superficial species) as the active and selective sites for CO conversion. Taking into account that when Cu° oligomeric sites are initially present, their oxidation under O_2 directly yields CuO at about 175°C (one single peak in the TPO curve), one should 'wait' higher temperature of about 200°C at which CuO is reduced into Cu_2O by H_2 (see TPR at Figure 8) to get the active sites. This last hypothesis is consistent with results from Choi et al who studied pre-reduced alumina supported copper and concluded that Cu^+ is the most active species among Cu°, Cu^+ and Cu^{2+} for CO oxidation [6]. A recent work investigating CuO/Cryptomolane effciciency in CO-PROX confirms that Cu^+ interfacial sites are active sites in CO oxidation [41]. In order to make this last hypothesis consistent with our PROX results obtained after an oxidizing pre-treatment, one should conclude that either Cu_2O oligomeric superficial sites already exist after such a treatment or that CO also

react with CuO oligomeric superficial sites. In the latter case, the Cu° oxidation into CuO would be the rate determining step of the overall CO oxidation mechanism.

3.6.2.3. Influence of the H_2 molar fraction.

In most of the PROX conditions, the amount of H_2 present in the reaction mixture is as high as possible in order to make the purified H_2 production at its highest value. That is the reason why the influence of the H_2 molar ratio was investigated. In the context of this study, the catalyst was submitted to an oxidizing pre-treatment in order to get the highest activity.

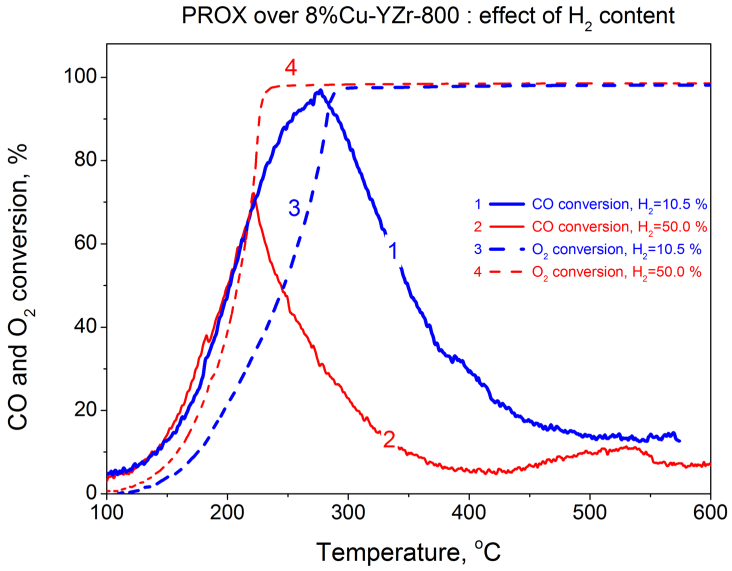

Figure 12: Study of the influence of the H_2 molar content in the PROX flow on the 8%Cu-YZr-800 catalytic efficiency. CO (solid curves 1, 2) and O_2 (dashed curves 3, 4) conversion obtained in PROX conditions made of 1 % CO, *x* H_2 and 1.5 % O_2 in Ar at GHSV = 10 000 h^{-1} and a heating rate of 5 $K.min^{-1}$. Curves 1, 3 and curves 2, 4 correspond to *x* =10.5% and 50%, respectively.

Figure 12 clearly reveals that as far as the temperature is kept below 200°C, an increase of the H_2 amount from 10.5% to 50% does not affect the CO conversion. Even if the O_2 conversion shift to lower temperature indicates a decrease of the O_2 selectivity toward CO_2, it is important to note that CO remains preferentially oxidized even in a high excess of H_2. The very fast decay of the CO conversion above T=200°C is to be related with the concomitant O_2 full conversion. In order to summarize the above results, it seems import to highlight that Cu sites highly selective towards CO oxidation are mostly involved for temperature below 200°C, while non selective oxidation sites become the dominant active sites at higher temperature making the O_2 consumption mostly involved in hydrogen oxidation.

4. Conclusions

In the present work, the original co-precipitation synthesis of YZr nanostructured oxides loaded with either 1 or 8 mol. % of copper was successfully achieved. Two distinct annealing temperatures of 600 °C and 800 °C were applied and XRD analyses together with HREM images proved that the tetragonal phase required for optimal catalytic efficiency was preserved up to 97% whatever the calcination temperature. On another side, high annealing temperature coupled with high Cu loading provokes the formation of several void cavities (about 10 nm) inside each single crystal. These cavities result form the out migration of excess copper towards the crystal external surface. As a consequence, samples calcined at high temperature not only present cupper sites inside the YZr framework (lattice sites) but also both highly dispersed Cu_xO_y oligomeric species and bigger CuO particles located at the outside surface, as evidenced by UV-Vis and TPR analysis.

PROX catalytic tests were then performed in a wide temperature range in order to test the O_2 selectivity towards CO_2 under severe conditions. Under the temperature programmed reaction conditions (10°C.min^{-1} heating rate) that were used, a CO conversion level as high as 95% was obtained at 260°C. The absence of catalyst deactivation was confirmed upon repeating the test under exactly similar conditions and without any pre-treatment. Identical CO and O_2 conversion curves were obtained indicating that our ceria free formulation is not sensitive to the CO_2 and H_2O reaction products.

Concerning the nature of the involved sites, it was found that copper lattice sites are not good candidate for catalytic sites active for CO oxidation in the low temperature range. Furthermore, it was shown that an increase of the annealing temperature from 600°C to 800°C clearly boosts the catalytic efficiency of sample loaded with 1% Cu. The copper lattice out diffusion most probably through interstitial sites thus provides the superficial active sites. Regarding the O_2 selectivity towards CO_2, a higher performance for the 1%Cu–YZr-800 catalyst was observed in the temperature range above 280°C at which the O_2 conversion reaches the 100% level for all samples. Indeed, for T>280°C, the CO conversion drops quickly to values lower than 20% (at about 400°C) for 8%Cu–YZr-800 while it decreases slowly and remains above 50% up to 600°C for 1%Cu–YZr-800. This behaviour together with the detection of CuO clustering by both UV-Vis and EDX profile at grain boundary for the 8%Cu–YZr-800 sample strongly suggest that the bigger the cupper oxide particles at the YZr surface, the less selective are the associated oxidation sites. This conclusion thus makes oligomeric copper superficial species the best candidate for the active and selective sites for CO oxidation. More precisely, a detailed analysis of the impact of either a reducing or oxidizing pre-treatment strongly supports that Cu_2O oligomeric superficial sites would be the selective ones for CO oxidation in the low temperature range.

Finally, the main goal of this study was achieved: thanks to the use of complementary analysis techniques associated with PROX efficiency tests, interesting relationships between superficial sites and catalytic activity/selectivity were obtained allowing to suggest relevant active sites.

Acknowledgements

This work was partly supported by the National Academy of Sciences of Ukraine as well as the Ministry of Education and Sciences of Ukraine (project 89452).

References

[1] T.V. Choudhary, D.W. Goodman, Catalysis Today 77 (2002) 65-78.

[2] E.D. Park, D. Lee, H.C. Lee, Catalysis Today 139 (2009) 280-290.

[3] S.G. Kandlikar, Z. Lu, Journal of Fuel Cell Science and Technology 6 (2009).

[4] R. Lan, X.X. Xu, S.W. Tao, J.T.S. Irvine, Journal of Power Sources 195 (2010) 6983-6987.

[5] K.H. Ng, H.A. Rahman, M.R. Somalu, International Journal of Hydrogen Energy 44 (2019) 30692-30704.

[6] K.I. Choi, M.A. Vannice, Journal of Catalysis 131 (1991) 22-35.

[7] N. Bion, F. Epron, M. Moreno, F. Marino, D. Duprez, Topics in Catalysis 51 (2008) 76-88.

[8] M. Haruta, CATTECH 6 (2002) 102.

[9] M. Angel Centeno, T.R. Reina, S. Ivanova, O. Hernando Laguna, J. Antonio Odriozola, Catalysts 6 (2016).

[10] S. Rousseau, O. Marie, P. Bazin, M. Daturi, S. Verdier, V. Harle, Journal of the American Chemical Society 132 (2010) 10832-10841.

[11] M. Kipnis, Applied Catalysis B-Environmental 152 (2014) 38-45.

[12] P. Lakshmanan, J.E. Park, E.D. Park, Catalysis Surveys from Asia 18 (2014) 75-88.

[13] A. Martinez-Arias, D. Gamarra, A.B. Hungria, M. Fernandez-Garcia, G. Munuera, A. Hornes, P. Bera, J.C. Conesa, A. Lopez Camara, Catalysts 3 (2013) 378-400.

[14] D. Gamarra, A.L. Cámara, M. Monte, S.B. Rasmussen, L.E. Chinchilla, A.B. Hungría, G. Munuera, N. Gyorffy, Z. Schay, V.C. Corberán, J.C. Conesa, A. Martínez-Arias, Applied Catalysis B: Environmental 130-131 (2013) 224-238.

[15] P.S. Barbato, A. Di Benedetto, G. Landi, L. Lisi, Topics in Catalysis 59 (2016) 1371-1382.

[16] A. Martínez-Arias, D. Gamarra, M. Fernández-García, A. Hornés, P. Bera, Z. Koppány, Z. Schay, Catalysis Today 143 (2009) 211-217.

[17] D. Gamarra, G. Munuera, A.B. Hungría, M. Fernández-García, J.C. Conesa, P.A. Midgley, X.Q. Wang, J.C. Hanson, J.A. Rodríguez, A. Martínez-Arias, The Journal of Physical Chemistry C 111 (2007) 11026-11038.

[18] P. Li, X. Chen, Y. Li, J.W. Schwank, Catalysis Today 327 (2019) 90-115.

[19] D. Devaiah, L.H. Reddy, S.-E. Park, B.M. Reddy, Catalysis Reviews-Science and Engineering 60 (2018) 177-277.

[20] A. Martínez-Arias, A.B. Hungría, M. Fernández-García, J.C. Conesa, G. Munuera, Journal of Power Sources 151 (2005) 32-42.

[21] M. Shimokawabe, H. Asakawa, N. Takezawa, Applied Catalysis 59 (1990) 45-58.

[22] R.-X. Zhou, X.-Y. Jiang, J.-X. Mao, X.-M. Zheng, Applied Catalysis A: General 162 (1997) 213-222.

[23] Z.-Y. Ma, C. Yang, W. Wei, W.-H. Li, Y.-H. Sun, Journal of Molecular Catalysis A: Chemical 231 (2005) 75-81.

[24] S.K. Tadokoro, E.N.S. Muccillo, Journal of Alloys and Compounds 344 (2002) 186-189.

[25] M.R. Alvarez, A.R. Landa, L.C. Otero-Diaz, M.J. Torralvo, Journal of the European Ceramic Society 18 (1998) 1201-1210.

[26] V.P. Pakharukova, E.M. Moroz, V.V. Kriventsov, T.V. Larina, A.I. Boronin, L.Y. Dolgikh, P.E. Strizhak, The Journal of Physical Chemistry C 113 (2009) 21368-21375.

[27] C.-C. Chao, J.S. Park, X. Tian, J.H. Shim, T.M. Gür, F.B. Prinz, ACS Nano 7 (2013) 2186-2191.

[28] N. Korsunska, M. Baran, I. Vorona, V. Nosenko, S. Lavoryk, X. Portier, L. Khomenkova, Nanoscale Research Letters 12 (2017) 157.

[29] N. Korsunska, M. Baran, Y. Polishchuk, O. Kolomys, T. Stara, M. Kharchenko, O. Gorban, V. Strelchuk, Y. Venger, V. Kladko, L. Khomenkova, ECS Journal of Solid State Science and Technology 4 (2015) N103-N110.

[30] N. Korsunska, Y. Polishchuk, M. Baran, V. Nosenko, I. Vorona, S. Lavoryk, S. Ponomaryov, O. Marie, X. Portier, L. Khomenkova, Frontiers in Materials 5 (2018).

[31] N. Korsunska, V. Papusha, O. Kolomys, V. Strelchuk, A. Kuchuk, V. Kladko, Y. Bacherikov, T. Konstantinova, L. Khomenkova, physica status solidi c 11 (2014) 1417-1422.

[32] R. Srinivasan, R.J. De Angelis, G. Ice, B.H. Davis, Journal of Materials Research 6 (2011) 1287-1292.

[33] A. Benedetti, G. Fagherazzi, F. Pinna, Journal of the American Ceramic Society 72 (1989) 467-469.

[34] N. Korsunska, Y. Polishchuk, V. Kladko, X. Portier, L. Khomenkova, Materials Research Express 4 (2017).

[35] M. Thommes, K. Kaneko, V. Neimark Alexander, P. Olivier James, F. Rodriguez-Reinoso, J. Rouquerol, S.W. Sing Kenneth, Physisorption of gases, with special reference to the evaluation of surface area and pore size distribution (IUPAC Technical Report), Pure and Applied Chemistry, 2015, p. 1051.

[36] J.P. Goff, W. Hayes, S. Hull, M.T. Hutchings, K.N. Clausen, Physical Review B 59 (1999) 14202-14219.

[37] V.P. Pakharukova, E.M. Moroz, D.A. Zyuzin, A.V. Ishchenko, L.Y. Dolgikh, P.E. Strizhak, The Journal of Physical Chemistry C 119 (2015) 28828-28835.

[38] A. Martínez-Arias, A.B. Hungría, M. Fernández-García, A. Iglesias-Juez, J. Soria, J.C. Conesa, J.A. Anderson, G. Munuera, Physical Chemistry Chemical Physics 14 (2012) 2144-2151.

[39] A. Martínez-Arias, A.B. Hungría, G. Munuera, D. Gamarra, Applied Catalysis B: Environmental 65 (2006) 207-216.

[40] M. Richard, F. Can, D. Duprez, S. Gil, A. Giroir-Fendler, N. Bion, Angewandte Chemie-International Edition 53 (2014) 11342-11345.

[41] A. Davó-Quiñonero, I. Such-Basáñez, J. Juan-Juan, D. Lozano-Castelló, P. Stelmachowski, G. Grzybek, A. Kotarba, A. Bueno-López, Applied Catalysis B: Environmental 267 (2020) 118372.